



THERMAL ANOMALIES PRIOR TO THE 2015 GORKHA (NEPAL) EARTHQUAKE FROM MODIS LAND SURFACE TEMPERATURE AND OUTGOING LONGWAVE RADIATIONS

M. Shah¹, M. Khan², H. Ullah³, S. Ali³

¹ Women University, Swabi, Pakistan

² University of Chinese Academy of Sciences, Beijing, China

³ Quaid-i-Azam University University, Islamabad, Pakistan

Abstract: Earthquakes can generate thermal anomalies in the atmosphere at low altitudes. Pending well-focused detailed studies, such phenomenon may be referred to as a precursor for earthquake prediction. However, today the pre-earthquake thermal anomalies are not clear enough. In this paper, the thermal anomalies prior to the April 25, 2015 Mw 7.8 Gorkha (Nepal) earthquake are investigated from the Moderate Resolution Imaging Spectroradiometer (MODIS) land surface temperature (LST), air temperature and Outgoing Longwave Radiations (OLR) data. The 2D and 3D wavelet transformation techniques are used to interpret the real time enhancement of the daily MODIS and OLR data before the impending earthquake. Using the wavelet density spectrum, pre-earthquake anomalies in MODIS and OLR are found in connection to the impending earthquake. The spatial images of MODIS and OLR show the evolutionary pattern of the emanation of ions from the epicenter and the surrounding area. The most important feature revealed by the spatial analysis is the eastward migration of temperature clouds due to a strong electric field. The satellite based LST data showed deviation, which crosses the upper bound by 5 °C. All the observations in our case study strongly support the notion of pre-earthquake thermal anomalies. Based on the analysis of the results, it can be concluded that the overabundance of ions from the seismogenic zone is responsible for prompting large temperature perturbations in atmospheric layers.

Key words: thermal anomaly; MODIS; earthquake; OLR; air temperature

RESEARCH ARTICLE

Handling Editor: V.A. Sankov

Received: October 3, 2017

Revised: January 17, 2018

Accepted: February 20, 2018

For citation: Shah M., Khan M., Ullah H., Ali S., 2018. Thermal anomalies prior to the 2015 Gorkha (Nepal) earthquake from MODIS Land Surface Temperature and Outgoing Longwave Radiations. *Geodynamics & Tectonophysics* 9 (1), 123–138. doi:10.5800/GT-2018-9-1-0341.

ТЕМПЕРАТУРНЫЕ АНОМАЛИИ ПЕРЕД ЗЕМЛЕТРЯСЕНИЕМ В ПРОВИНЦИИ ГОРКХА (НЕПАЛ) В 2015 Г., УСТАНОВЛЕННЫЕ ПО ЗНАЧЕНИЯМ ТЕМПЕРАТУРЫ ПОВЕРХНОСТИ ЗЕМЛИ MODIS И УХОДЯЩЕГО ДЛИННОВОЛНОВОГО ИЗЛУЧЕНИЯ

М. Шах¹, М. Хан², Х. Уллах³, С. Али³

¹ Университет для женщин, Сваби, Пакистан

² Университет Китайской академии наук, Пекин, Китай

³ Университет Кауд-и Азам, Исламабад, Пакистан

Аннотация: Землетрясения способны создавать тепловые аномалии в атмосфере на малых высотах. Такие аномалии могут рассматриваться в качестве вероятного предвестника при прогнозировании землетрясений, в связи с чем требуются целенаправленные детальные исследования. На сегодня знаний о тепловых аномалиях, появляющихся перед землетрясениями, недостаточно. В статье представлены результаты изучения термических аномалий, имевших место перед землетрясением в провинции Горкха (Непал) ($M_w=7.8$) 25 апреля 2015 г., как свидетельствуют значения температуры поверхности Земли, зарегистрированные сканирующими спектрорадиометрами среднего разрешения MODIS, а также данные о температуре атмосферного воздуха и уходящего длинноволнового излучения (OLR). Метод вейвлет-преобразования в двух- и трехмерном пространстве использован для интерпретации повышения суточных значений MODIS и OLR в реальном времени накануне землетрясения. По спектральной плотности накануне реального сейсмического события установлены аномальные значения MODIS и OLR, связанные с приближением этого землетрясения. Пространственные снимки MODIS и OLR показывают эволюционирующий характер эманации ионов из эпицентра и прилегающей области. Наиболее важной особенностью, выявленной посредством пространственного анализа, следует считать миграцию температурных облаков в восточном направлении вследствие усилившегося электрического поля. Спутниковые данные LST показывают отклонение от верхней границы значений на 5 °C. Все наблюдения в нашем исследовании подтверждают понятие тепловых аномалий накануне землетрясения. Исходя из анализа результатов, можно сделать вывод, что избыток ионов из сейсмогенной зоны обуславливает появление больших температурных возмущений в слоях атмосферы.

Ключевые слова: термическая аномалия; MODIS; землетрясение; OLR; температура атмосферы

1. INTRODUCTION

Among the remarkable phenomena that have been widely reported to occur prior to major earthquakes are anomalies in the thermal infrared (TIR) emission from the ground [Tronin et al., 2004; Saradjian, Akhoondzadeh, 2011]. These anomalies are typically observed a few days to a week or two weeks before the main shocks and may linger on into the aftershock period. They have traditionally been explained by warm gases emanating from the ground, due to micro-fracturing of rocks and opening of fissures [Freund, 2010].

However, inconsistencies with this explanation have been noted early. In many cases, even though the epicenters of the seismic events and the active faults were located on flat land or in valleys, the observable TIR emissions were concentrated on topographic highs or mountains some distance from the epicenter locations [Piroddi et al., 2014b]. Three examples among many are the TIR anomalies preceding the 14 October 2004

Mw 5.1 (Raver, Iran), the 22 July 2007 M 5.0 (Yamnotri, India), and the 19 January 2011 M 7.2 (Dalbandin, Pakistan) earthquakes [Saraf et al., 2008]. Another striking example, for which TIR maps with high temporal and spatial resolution are available, is the 06 April 2008 M6.3 L'Aquila earthquake (Italy) [Piroddi et al., 2014a, 2014b]. Figure 1a in Piroddi et al. [2014b] shows the satellite images of the L'Aquila valley and the surrounding area. The valley floor is known to have been dissected by several active faults, including the one that ruptured during the L'Aquila event. Hence, the valley floor can be viewed as the most likely place wherein warm gases could have emanated from the ground prior to the earthquake. However, according to Figure 1b, three nights before the earthquake, there was a very little excess TIR emission from the valley floor, while the mountain ranges on either sides exhibited strong TIR anomalies. Observations like these indicate that some of the ideas promoted since the discovery of TIR anomalies ($M_w=7.8$ Gorkha, Nepal) cannot be correct

and that the concept of warm gases or greenhouse gases seeping out of the ground at or near the fault zones prior to earthquakes has to be revised.

Different anomalous phenomena regarding the physical and chemical characteristics of pre-earthquake anomalies in the vicinity of earthquake breeding zones have been reported over the years, requiring a multi-disciplinary approach [Zhang *et al.*, 2009; Jin *et al.*, 2010, 2015; Liu *et al.*, 2009]. Their explicit relationships to the seismic events are often not clear. It has been proposed that energy released before major earthquakes can generate thermal anomalies in the lower atmosphere [Shah, Jin, 2015]. If so, these thermal anomalies must be due to a combination of complex chemical and physical processes caused by the stress in the rocks below the epicentral area. The recent studies of atmospheric precursors and their relation to earthquakes have been based on ground and satellite data [Piša *et al.*, 2011; Zhang *et al.*, 2009]. Several hypotheses and coupling models have been proposed to explain the lithosphere-atmosphere-ionosphere system and its possible mechanisms.

It has been suggested that, in the earthquake breeding region, the build-up of stresses in the rocks create fractures and fissures that would allow deep gases to seep out of the rocks and emanate into aquifers or ground water or the low-altitude atmosphere. These emanating gases would combine with gases that are already present, increasing the lithospheric pressure, raising up to atmosphere along the faults, and causing a temperature increase in the atmosphere. At the same time, water vapor would be released absorbing in the infrared as indicated by changes in the MODIS LST and unusual OLR data [Xiong *et al.*, 2010; Rawat *et al.*, 2011]. Pulinets *et al.* [2006b] reported that doubling of the volume of greenhouse gases would lead to a 5 °C increase in land surface temperatures injecting excess energy into the atmosphere. Concurrently, groundwater and spring waters in the epicentral regions have been reported to exhibit abnormally high concentrations of CO₂ and to undergo other chemical changes prior to major earthquakes [Pulinets, Ouzounov, 2011].

While many of the explanations for the observable non-seismic pre-earthquake phenomena that have been offered in the literature appear plausible, it is to be noted that they are by no means universally accepted. There is opposition in some expert circles, in particular among seismologists [Freund, 2003; Freund *et al.*, 2007], who point out that the various components of the proposed lithosphere-atmosphere-ionosphere coupling are linked together by ad hoc postulates for which there is no observational confirmation. This is particularly true for the assumption that, prior to major earthquakes, fissures would open in the shallow crust, from where gases can emanate, which creates fresh fracture surfaces affecting the chemistry of groundwa-

ter and spring waters. The counterargument presented is primarily based on the observation that strain measurements in the shallow crust, using very sensitive strain gauges in boreholes up to 2 km depth or deeper, have been unable to confirm that a stress build-up at these levels would be high enough to cause fissuring and fracturing of the rocks [Freund, 2000]. Such observations invalidate an important tenet on which the most widely promoted lithosphere – atmosphere – ionosphere coupling ideas are based, namely that of pervasive pre-earthquake fissuring and fracturing of the rocks as a prerequisite for the release of gases from the ground and for changes in water chemistry. In addition, observations as documented in Figure 1a/b in Piroddi *et al.* [2014b] disprove the idea that the release of warm gases or greenhouse gases from the ground could be the cause of TIR anomalies.

Of course, earthquakes are mechanical events, during which enormous amounts of mechanical energy can be released within a very short time. It is reasonable to assume that, prior to such a process, stresses must build up in the hypocentral region deep below, where the catastrophic rupture will eventually occur when the stresses exceed a critical value. However, it is not reasonable to assume that, because earthquakes are mechanical events, all pre-earthquake phenomena must also be explicable on the basis of purely mechanical consequences of the build-up of stresses in the hypocenter and beyond such as fissuring and fracturing of the rocks in the shallow crust.

In this study, pre-earthquake thermal anomalies at high elevation areas associated with the 2015 Gorkha (Nepal) earthquake are studied and discussed, using the MODIS land surface temperature and OLR data.

2. OBSERVATION DATA AND METHODS

2.1. OBSERVATION DATA

The data of MODIS land surface temperature (LST), OLR and air temperature related to the 2015 Gorkha Mw 7.8 earthquake were retrieved from NASA/AVHRR and National Centers for Environmental Prediction (NCEP), respectively. Additionally, information about the seismicity, epicenter and moment magnitude of the earthquake was collected from the Global Centroid Moment Tensor Catalog (GCMT). This earthquake occurred on 25 April, 2015 at 06:11:25 (UTC). The epicenter was located 82.4 km NW of the capital city Kathmandu. Some information about the local geology and atmospheric conditions in the study area was obtained from the reports of the Meteorological Department of Nepal.

The Moderate Resolution Imaging Spectroradiometer (MODIS) sensor was designed in the mid-1995 to

monitor the Earth's atmosphere and launched in 1999 by the National Aeronautics and Space Administration (NASA) on two satellites, Terra and Aqua (originally named EOS AM-1 and EOS PM-1, respectively) orbiting at 705 km above the mean sea level. The MODIS instruments on the Aqua (ascending node) and Terra (descending node) satellites, operating on the sun-synchronous, near-polar circular orbit, survey the entire Earth's surface in 36 spectral bands ranging in wavelengths from 0.4 μm to 14.4 μm with 250 m, 500 m, and 1 km spatial resolutions. The MODIS footprint is 2330 km (cross track) by 10 km (along track at nadir). The data are combined into images that are publicly available on (<http://modis.gsfc.nasa.gov/data/>).

The Land Surface Temperature (LST) product based on thermal bands was averaged to check for dynamical changes in LST before the Mw 7.8 earthquake.

The Outgoing Long Wave Radiation (OLR) dataset is calculated from the infrared data (10–12 μm) collected by polar-orbiting satellites operated by the National Oceanic and Atmospheric Administration (NOAA). The spatial resolution for OLR is $2.5 \times 2.5^\circ$ (longitude \times latitude) for a single day. The OLR retrieving method described by Liebmann [1996] provides information about the Earth's atmosphere. When pre-earthquake OLR anomalies occur, they are thought to be caused by an unbalanced heat exchange between earthquake breeding zones and the air column. The main drivers of the OLR anomalies are thought to be gases and water vapor emanating from the ground in pre-seismic regions, though questions how coupling between the earth surface and the top of the atmosphere is supposed to have not been addressed yet.

Operationally, OLR is a useful parameter to estimate the variations in atmospheric conditions as related to pre-earthquake and earthquake activity. Changes in the OLR data are consistent with changes in other atmospheric parameters. Further information can be downloaded from the official website of NOAA Climate Prediction Center and NCEP Data Center, where the algorithm to calculate OLR and relevant publications are also available.

The Earth surface temperatures at Kathmandu and Pokhara were derived to confirm the MODIS land surface temperature perturbations. Based on emissivity, anomalous ground temperature increases up to 5–10 $^\circ\text{C}$ were recorded. According to [Saradjian, Akhoondzadeh, 2011; Akhoondzadeh, 2012], such increases in the ground temperature cannot be caused by any other known mechanism operational in the air, such as winds, storms or human activities. Meteorological stations in Kathmandu and Pokhara located near the epicenter provided the reference data and all the information used in our analysis of the temperature variations over the study area. The area investigated using statistical formulae covers the epicenter and the two

cities. Seismological information for Nepal was retrieved from USGS. The magnitudes, depths and moment tensors shown on the map of Nepal (Fig. 1) are given in (Table 1).

2.2. METHODS

In our study, the daily MODIS land surface temperature, OLR and air temperature values were analyzed in their confidence intervals ($\mu + 2\sigma$), which were calculated from the continuous data of 3 months before and after the observed day, where μ and σ indicate the mean and standard deviation of a normal distribution. This calculation method, widely applied in contemporary research [Akhoondzadeh, 2012; Saradjian, Akhoondzadeh, 2011], was used in our study to find temporal variations beyond the confidence interval.

Further, to better identify the right anomaly prior to the earthquake, the method based on wavelet transformation in 2D and 3D spectra was employed to find the real fluctuation in the MODIS and OLR data. This method provides for proper filtering out of noises and detects underlying perturbations. It is often noted that some anomalies in MODIS and OLR can be caused by space weather conditions. The main purpose of applying the wavelet transformation is to identify the effects of earthquake perturbations directly over the epicenter. Following [Akhoondzadeh, 2012; He et al., 2014], the governing equation of continuous wavelet transformation is:

$$W(u, s) = \frac{1}{\sqrt{s}} \int_{-\infty}^{+\infty} f(t) \psi^* \left(\frac{t-u}{s} \right) dt, \quad (1)$$

$$W(u, s) = W_R(u, s) + iW_I(u, s), \quad (2)$$

where W is comprised of real and imaginary parts, u and s are the translation and dilation parameters, respectively. The real and imaginary parts are expressed as:

$$\begin{cases} W_R(u, s) = \frac{1}{\sqrt{s}} \int_{-\infty}^{+\infty} f(t) \psi_R \left(\frac{t-u}{s} \right) dt \\ W_I(u, s) = -\frac{1}{\sqrt{s}} \int_{-\infty}^{+\infty} f(t) \psi_I \left(\frac{t-u}{s} \right) dt. \end{cases} \quad (3)$$

The most important goal was to discover local anomalies that had occurred prior to the earthquake. Unrelated, hence “false” signals may arise from other sources such as space weather conditions, which may influence the atmosphere at sometimes unexpected scales. It is mandatory in the wavelet transformation to apply the cross wavelet transformation. This stage basically assesses if the signal is caused by the earthquake dynamics or by any other geological processes. The mathematical form is:

$$W^{XY}(u, s) = W^X(u, s)W^{Y*}(u, s). \quad (4)$$

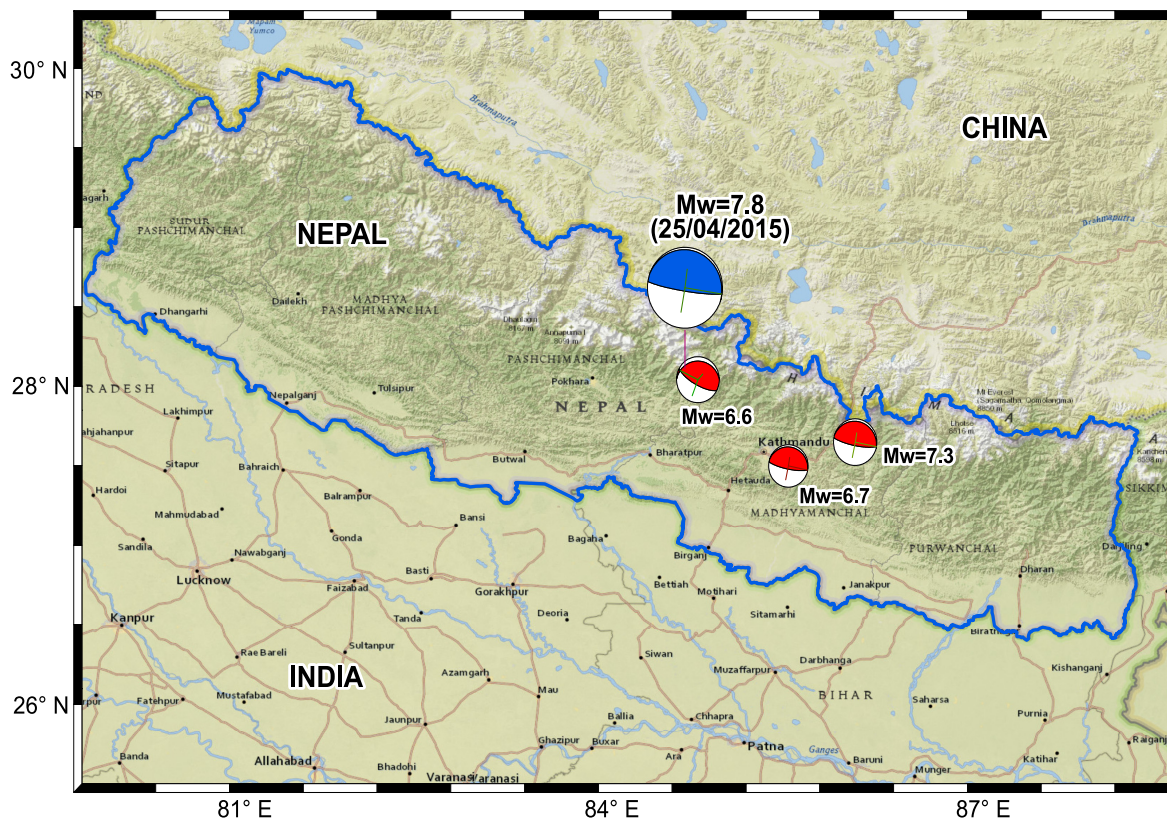


Fig. 1. Geographical location of the Mw 7.8 earthquake epicenter (shown by the blue-and-white beach ball). The small red-and-white balls show the Mw>6.5 aftershocks. Source: Table 1.

Рис. 1. Географическое положение эпицентра землетрясения Mw=7.8 (показано сине-белым кружком). Красно-белыми кружками показаны афтершоки Mw> 6.5. См. данные в таблице 1.

Equation (4) has a pair of complex conjugate terms, where $W^{Y*}(u, s)$ is complex conjugate of $W^Y(u, s)$. In addition, it is the representation of a cross wavelet power spectrum $W^{XY}(u, s)$. According to equation (4), if two temporal data sets are mutually correlated, their cross wavelet power spectrum would show a high energy region as compared to an ordinary region within the same spectrum [Cao, Qiao, 2008]. An anomaly is indicated by a mutual isolation of the imaginary part from

the real part of a continuous spectrum. In this part, the instantaneous time domain data are converted to the frequency domain by adding a wavelet factor [Grinsted et al., 2004]. After this conversion, a vanishing application is introduced in the form of an optimal mother wavelet. The mother wavelet not only enhances the resolution of real anomalies, but also removes residuals from the data. There are wavelets available in the MATLAB user environment. In our study, we used

Table 1. Earthquake catalogue based on the USGS data

Таблица 1. Каталог землетрясений по данным USGS

Date	Lat (°N)	Lon (°E)	Depth, km	Mw	Strike	Dip	Rake
April 18, 2015	27.01	83.51	25.6	4.9	306	77	92
April 21, 2015	28.65	82.35	26.4	5.0	118	44	66
April 25, 2015*	27.96	83.55	12.0	7.8	287	6	96
April 25, 2015	27.86	84.93	10.0	6.1	284	12	94
April 25, 2015	28.06	84.82	10.8	6.6	271	21	94
April 25, 2015	27.61	84.96	15.0	5.1	201	40	93
April 26, 2015	27.61	86.96	22.9	6.7	285	12	94

Note. * – the devastating earthquake of Mw=7.8.

Примечание. * – разрушительное землетрясение Mw=7.8.

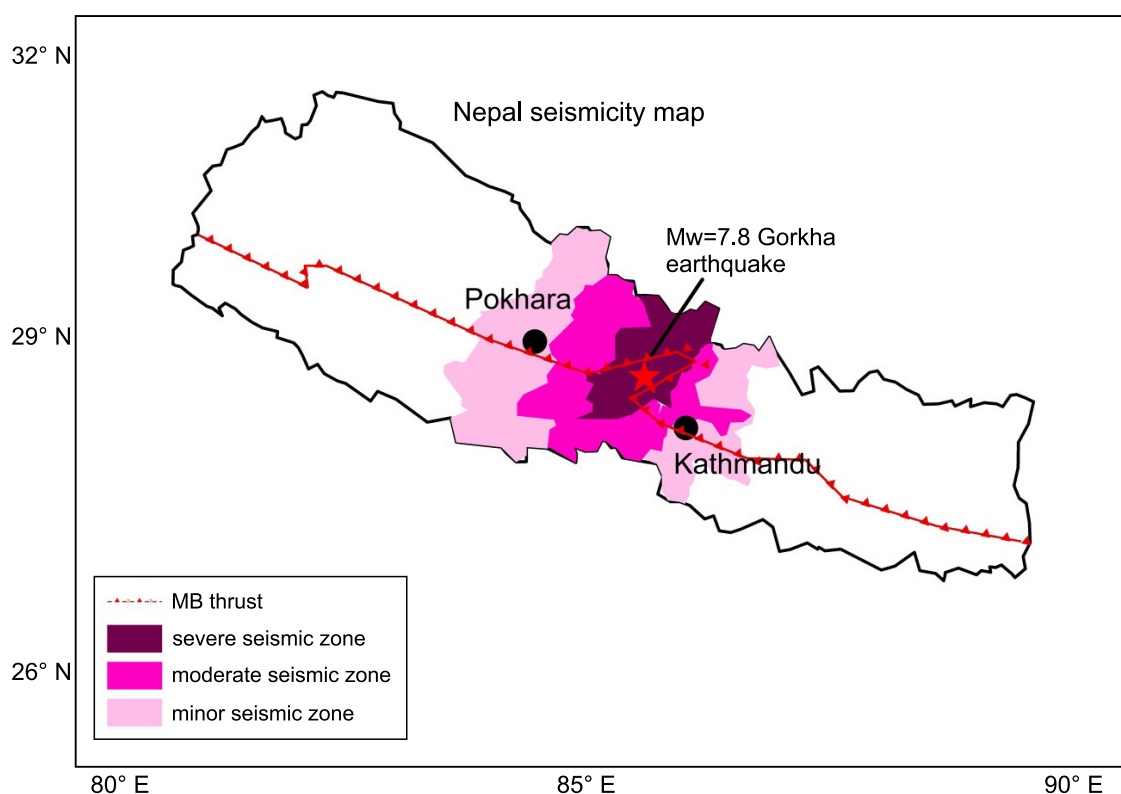


Fig. 2. A simplified scheme of seismicity in the study area. The red star shows the epicenter, and two black circles mark the areas observed by the Pokhara and Kathmandu Meteorological Stations. The Mw 7.8 epicenter is in the severe seismic zone, according to the United States Geological Survey (USGS).

Рис. 2. Схема сейсмичности в регионе исследований. Красной звездочкой отмечен эпицентр землетрясения; черными линиями очерчены области, где ведут наблюдения метеорологические станции в г. Покхара и г. Катманду. Эпицентр Mw=7.8 находится в зоне повышенной сейсмической активности, согласно данным Геологической службы США (USGS).

a wavelet named ‘gaus2’ belonging to the Gaussian family.

While implementing this method on the MODIS and OLR data, the real anomalies are highlighted as a case study for the Mw 7.8 earthquake. It is representative of unusual phenomena preceding the impending earthquake. The density spectrum is used to correlate the original time series with the daughter wavelets over a defined scale. The anomaly is found leading to the identification of the suspected MODIS and OLR days. Finally, the wavelet transformation provides an appropriate and defensible approach to characterize the variability in MODIS and OLR as due to an earthquake precursor and not due to other geophysical events/phenomena.

3. RESULTS AND DISCUSSION

The 25 April 2015 Mw 7.8 Gorkha earthquake (geographical coordinates 28.2°N, 84.6°E; geomagnetic coordinates 19.05°N, 158.81°E) hit the area near Kathmandu causing widespread loss of life and infrastructure. Due to its shallow depth and high magnitude, it

perturbed the nearby regions along the fault line known as the Main Boundary thrust (MBT). The National Disaster Management Authority of Nepal declared this earthquake the most devastating in the decade. Such catastrophic natural disasters are not infrequent in the Kathmandu valley due to the continuing collision of the Indian subcontinent with the Eurasian Plate. The region of Nepal between 26°N to 30°N and 80°E to 88°E is classified into different zones of seismicity. Figure 2 indicates the different seismic zones of Nepal, where the epicenter of Mw=7.8 is in the high seismicity portion. As part of this study, we find that this seismic concentration is mirrored in the atmosphere, which reinforces our contention that the MODIS and OLR anomalies are indeed precursors to the Mw 7.8 earthquake. Thus, it is important to understand the coupling between the ground data and the observables derived from the satellite data.

3.1. MODIS ANALYSIS

In this study, the MODIS LST and OLR datasets were analyzed both spatially and temporally to quantify the

Table 2. Enhancement in the MODIS LST, OLR and air temperature

Таблица 2. Повышение значений MODIS LST, OLR и температуры атмосферного воздуха

Parameters	Date	Value above mean
Compilation of temporal analysis		
Air temperature in Pokhara	20 April 2015	7 °C
Air temperature in Kathmandu	20 April 2015	5 °C
MODIS LST	20 April 2015	13 °C
OLR	21 April 2015	11 W/m ²
Compilation of spatial analysis		
MODIS LST	20 April 2015	10–15 °C
OLR	21 April 2015	-7 W/m ²

perturbation in the lower atmosphere before the earthquake in the study region. The perturbations in MODIS LST, OLR and air temperature are compiled in Table 2. However it is necessary to discuss the characterization of each parameter individually. As shown in Fig. 3, the MODIS LST and air temperature had high deviations of more than 5 °C on 20 April 2015 before the impending earthquake. The MODIS LST images of the area within 26–30° north and 80–88° east were averaged to analyze the seismogenic region. Then, the up-

per and lower bounds in the form of mean and standard deviations ($\mu \pm 2\sigma$) were calculated for the normal distribution of LST to understand the instantaneous changes occurring prior to the earthquake. After implementing the statistical window of the confidence interval, a prominent thermal infrared anomaly in the reported air temperature data of Pokhara and Kathmandu can be noted 5 days before the earthquake. The anomaly is beyond the upper bound of 5 °C, which is very unusual. The LST and air temperature anomalies

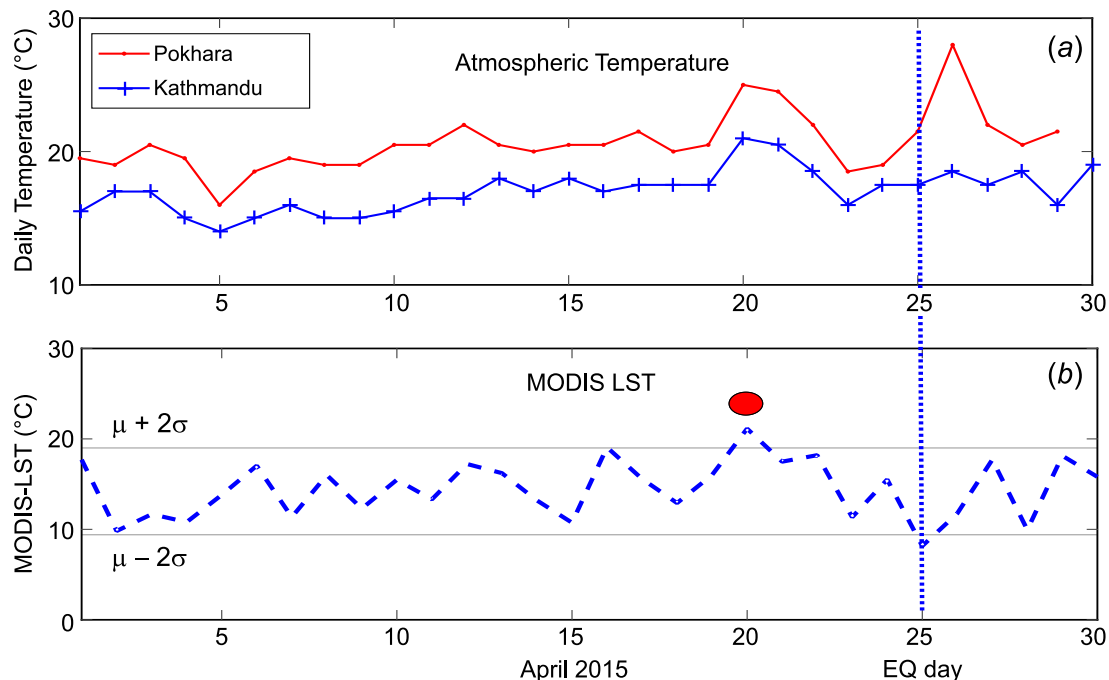


Fig. 3. Atmospheric temperature values recorded by the nearby meteorological stations, which were used to detect an enhancement of air temperature related to the Mw 7.8 earthquake (a). The daily average MODIS (LST) against the dates showing a significant perturbation on 20 April 2015, i.e. 5 days before the Mw 7.8 earthquake (b).

Рис. 3. Значения температуры атмосферы, зарегистрированные метеорологическими станциями, расположенными неподалеку от эпицентра землетрясения (а). По этим данным выявлено повышение температуры атмосферного воздуха в связи с землетрясением Mw=7.8. Среднесуточные значения MODIS (LST), указанные по датам, свидетельствуют о значительном возмущении 20 апреля 2015 г., т.е. за 5 дней до землетрясения Mw=7.8 (б).

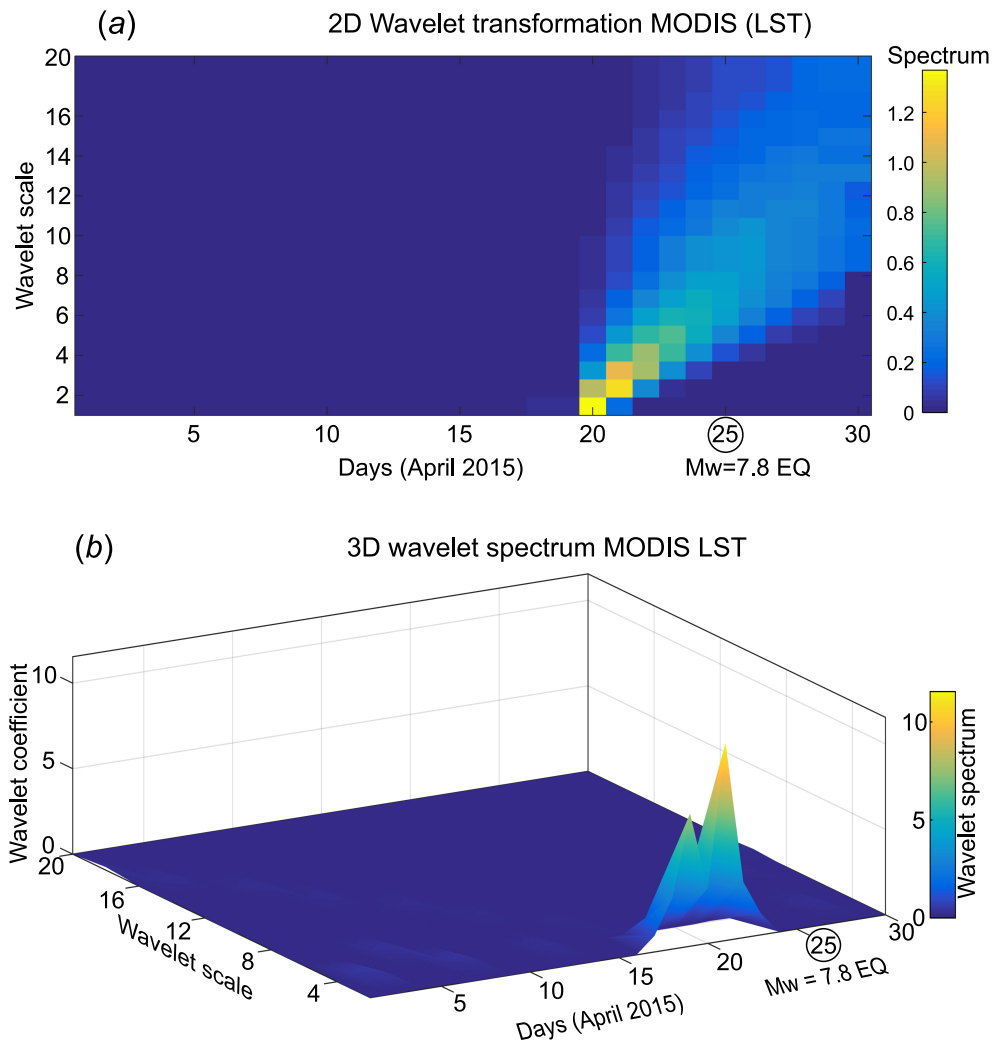


Fig. 4. MODIS LST data examined by wavelet transformation. The instantaneous wavelet density spectrum of MODIS LST using “guas2” wavelet (the earthquake date is shown by the circle) (a). The 3D wavelet spectrum with the same mother wavelet for Mw=7.8 on 25 April 2015 (b).

Рис. 4. Значения MODIS LST, проанализированные с применением метода вейвлет-преобразования. Спектр плотности всплесков MODIS LST с использованием вейвлета «guas2» (дата землетрясения обведена кружком) (а). Трёхмерный вейвлет-спектр с одним и тем же исходным вейвлетом для Mw=7.8 (25 апреля 2015 г.) (б).

occur at the same local time, indicating an unusual temperature behavior both in the land surface and the lower atmosphere, which appears to be related to the impending earthquake. According to [Saradjian, Akhoondzadeh, 2011], MODIS LST and air temperature anomalies may come from the same source, but their mechanisms must be different. In fact, what these mechanisms are and how they differ is still not clear. Variations in topography and geophysical conditions in the area, as well as latitudinal variations may cause such anomalies. To detect the LST anomaly before the impending earthquake, the wavelet transformation was applied. According to The energy density spectrum in Figs. 4a and 4b show that 20 April 2015 is marked by high values and reveals enhancements of two types, with the analytic wavelet transform (AWT) and the

cross-wavelet transform (XWT) both exhibiting the same effect, obviously due to the impending earthquake. The LST enhancement is higher in the afternoon as shown in Fig. 4b. Our data do not include variations of other geophysical events, which were found to be insignificant. In addition to the MODIS LST, the air temperature in the vicinity of the epicenter is also perturbed, which may be an indicator of pressure, temperature and humidity influenced by small ions [Liperovsky et al., 2005; Saraf et al., 2008]. These thermal anomalies could also be due to the impending earthquake. Atmospheric variations caused by other geophysical events are negligible.

To provide a stringent proof for the relationship of MODIS LST to the Mw 7.8 earthquake, the spatial images were used. We obtained the normal temperature

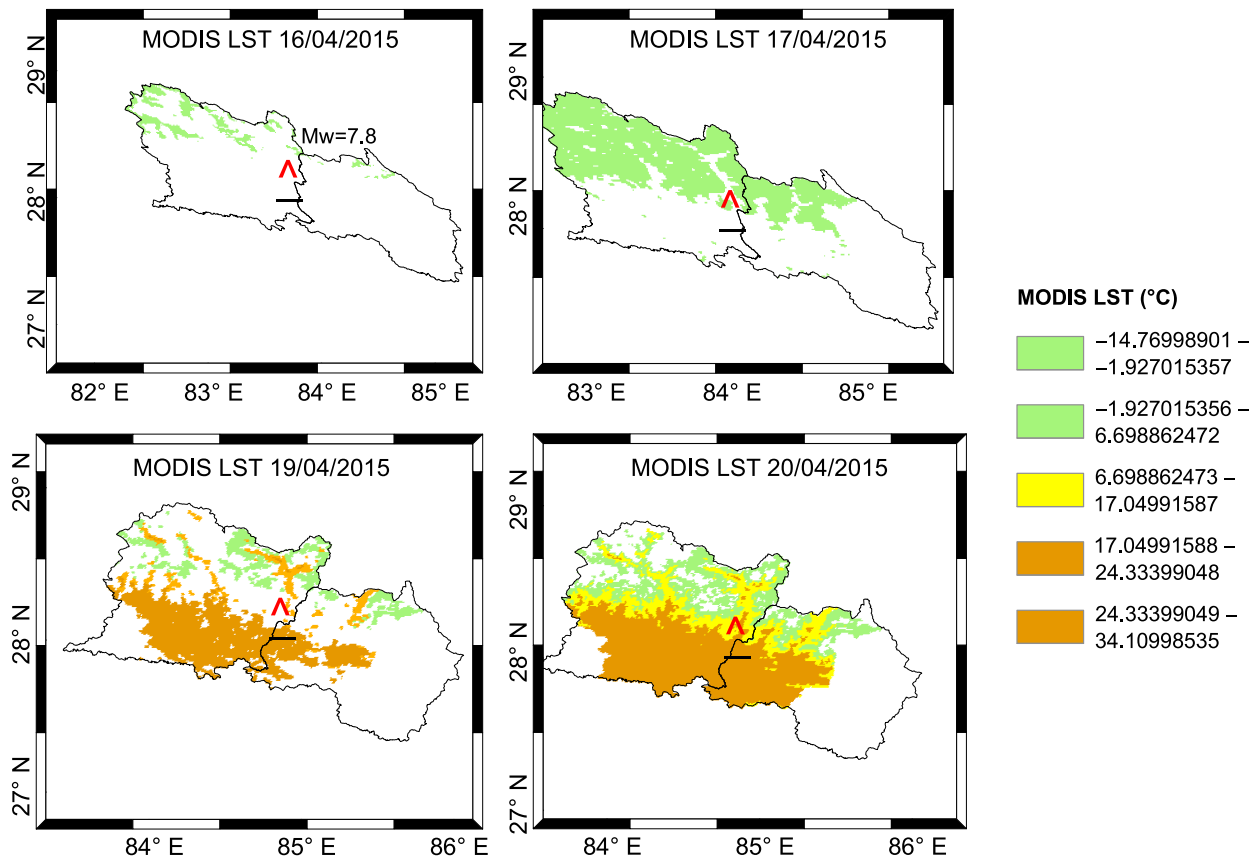


Fig. 5. Spatial images of MODIS Land surface temperature prior to the Mw 7.8 earthquake on the local scale. The images are in the chronological order from the 17th to 20th of April 2015. The red star marks the Mw 7.8 earthquake epicenter. The legend shows the cluster of surface temperature over the earthquake breeding zone.

Рис. 5. Пространственные снимки температуры поверхности Земли MODIS накануне землетрясения Mw=7.8. Изображения приведены в хронологическом порядке с 17-го по 20-е апреля 2015 г. Красной звездочкой отмечен эпицентр землетрясения Mw=7.8. Условным обозначением показан кластер значений температуры поверхности Земли над зоной подготовки землетрясения.

in °C for the MODIS Land Surface Temperature. The sinusoidal map projection of LST images was converted to specific geographic latitude/longitude under the Datum WGS-84 platform. The resolution of each pixel was enhanced to 500 times by performing this step [Jianxi *et al.*, 2008, and references therein].

In this study, the spatial images of both local and regional areas were examined to interpret the temperature maxima over the epicenter region. The images for the 16th, 17th, 19th and 20th of April 2015 were further analyzed to monitor the path of thermal anomalies. In order to focus on the coupling system, the MODIS LST images were analyzed on both the local and regional levels.

Pulinets and Ouzounov [2011] examined the characteristics of radon emission in seismically active regions, positing that a radon release increases the LST due to vertical electric fields, ultimately causing thermal anomalies. They explained the mechanism, how radon creates vertical electric fields and how those fields can

cause thermal anomalies. In our paper, Fig. 5 shows an anomalous temperature variation on 19 April 2015 along a line from Pokhara to Kathmandu with the epicenter roughly halfway. This anomaly spreads out over a very large area, the whole southern portion of Nepal as shown in Fig. 6. Although this phenomenon is consistent with the eastward drift of atmospheric winds prior to the earthquake, it is burdened by many uncertainties. A cluster of high temperature values is detected over the epicenter on 20 April 2015 on both the local and regional images. Its size is $5 \times 3^\circ$ (longitude \times latitude), i.e. 556 km \times 228 km. This anomaly traveled eastwards, which confirms its highly dynamic nature.

3.2. OLR OBSERVATIONS

In order to be fully confident about the existence of atmospheric precursors before the Mw 7.8 Nepal earthquake, the OLR data were analyzed in combination with the MODIS LST and air temperature data. The

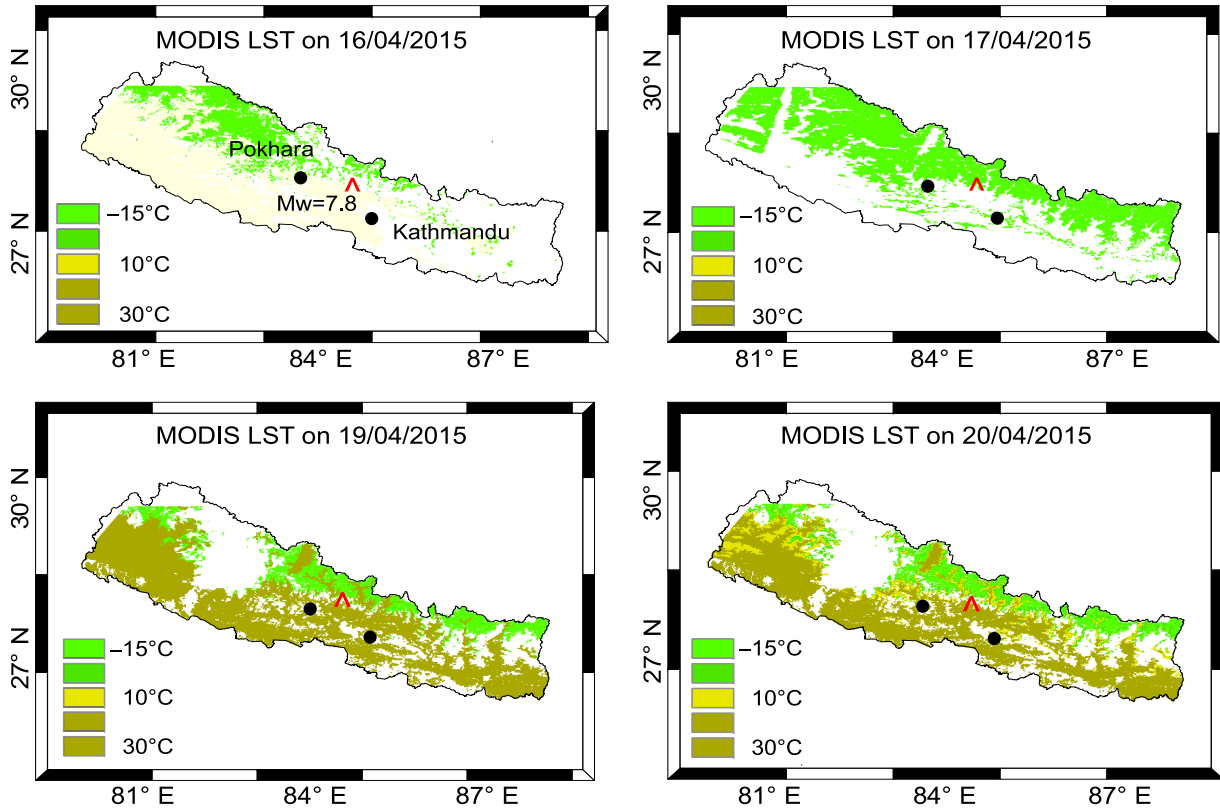


Fig. 6. Spatial images of MODIS for Nepal from the 17 to 20 of April 2015. The red star marks the Mw 7.8 earthquake epicenter. The two black circles show the locations of the nearby meteorological stations in Pokhara and Kathmandu.

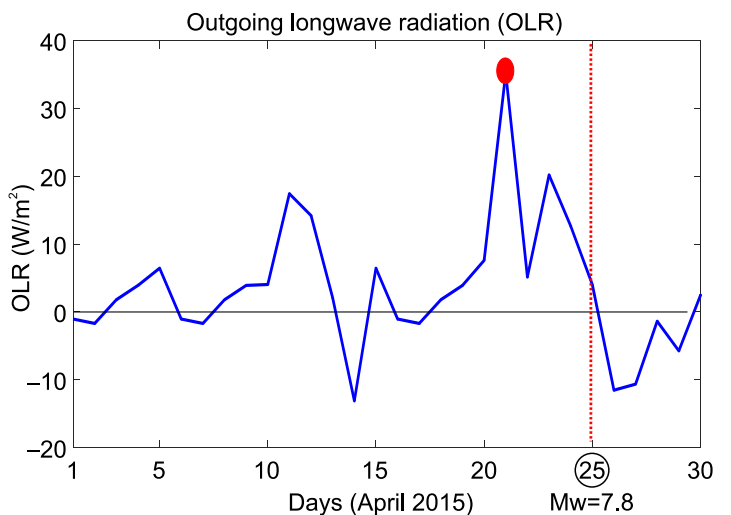
Рис. 6. Пространственные снимки MODIS для территории Непала с 17 по 20 апреля 2015 г. Красной звездочкой отмечен эпицентр землетрясения ($M_w=7.8$); две черные точки показывают места расположения метеорологических станций в г. Покхара и г. Катманду.

OLR data included information about the thermal radiation emitted from the lithosphere to the atmosphere. Thus it is appropriate to calculate the abnormal ground radiation before the earthquake. We studied the daily OLR grid $2.5 \times 2.5^\circ$ (longitude \times latitude) as a function of

time relative to the earthquake day. The statistical methods detected the anomalous OLR values on 21 April 2015 (Fig. 7), which coincided with the anomaly in the MODIS LST data. This correlation between OLR and MODIS LST confirms that the transfer of energy

Fig. 7. Vulnerable OLR value over the Mw 7.8 earthquake epicenter (28.2°N , 84.6°E). The earthquake date is show in a circle and marked by the red vertical line. The OLR values are shown along the y-axis. The dates are shown along the x-axis.

Рис. 7. Уязвимое значение OLR над эпицентром землетрясения $M_w=7.8$ (28.2° с. ш., 84.6° в. д.). Дата землетрясения обведена кружком и отмечена красной вертикальной линией. Значения OLR показаны по оси y. Даты показаны по оси x.



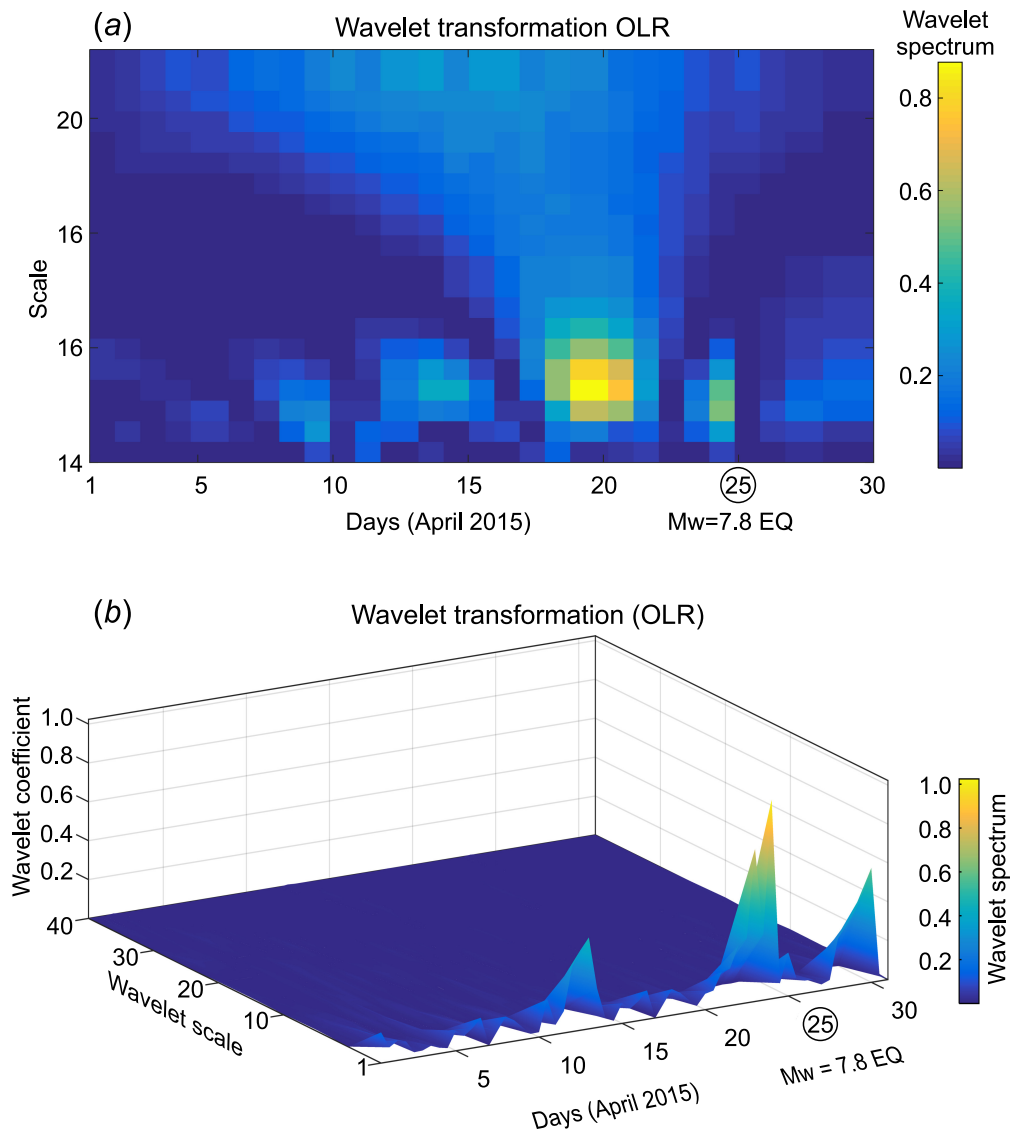


Fig. 8. OLR data examined by the wavelet transformation. (a) – the wavelet density spectrum of OLR using “guas2” wavelet. The earthquake date is marked by a circle. (b) – the 3-D wavelet transformation with the same mother wavelet for Mw=7.8 on 25 April 2015.

Рис. 8. Значения OLR, проанализированные с применением метода вейвлет-преобразования. (a) – спектр плотности всплесков OLR с использованием вейвлета «guas2». Дата землетрясения обведена кружком. (b) – трехмерный вейвлет-спектр с одним и тем же исходным вейвлетом для Mw=7.8 (25 апреля 2015 г.).

from the ground to the atmosphere as caused by processes linked to the impending earthquake. It shows that the atmosphere is sensitive to short term earthquake precursors. As depicted in Fig. 8a and 8b, wavelet transformation was applied to the OLR data to bring out the pre-earthquake anomaly. It shows that the anomaly on April 21st is 5 units greater than the anomaly near the earthquake date. Such an extremely large anomaly gives evidence of the advantage of the wavelet transformation analysis. The density spectrum values are large close to the earthquake date, indicating that, indeed, a relation exists between the OLR anomaly and the earthquake as illustrated in Fig. 8b.

The OLR results were further validated by investigating the daily images obtained from NCEP (National Centers for Environmental Prediction, USA). We used the method described in [Pulinets *et al.*, 2006b; Qin *et al.*, 2012] to acquire the OLR data as shown in Fig. 9. A significant OLR anomaly is seen to hover over the earthquake breeding zone with maximal values. The OLR anomaly of April 21st followed the path of the fault line and it is a clue to the impending earthquake. It is also evident that the OLR anomaly moved along the fault line from April 19th to April 22nd. A possible cause for this drift could be the strong wind in the seismogenic region, which was able to carry airborne ions in

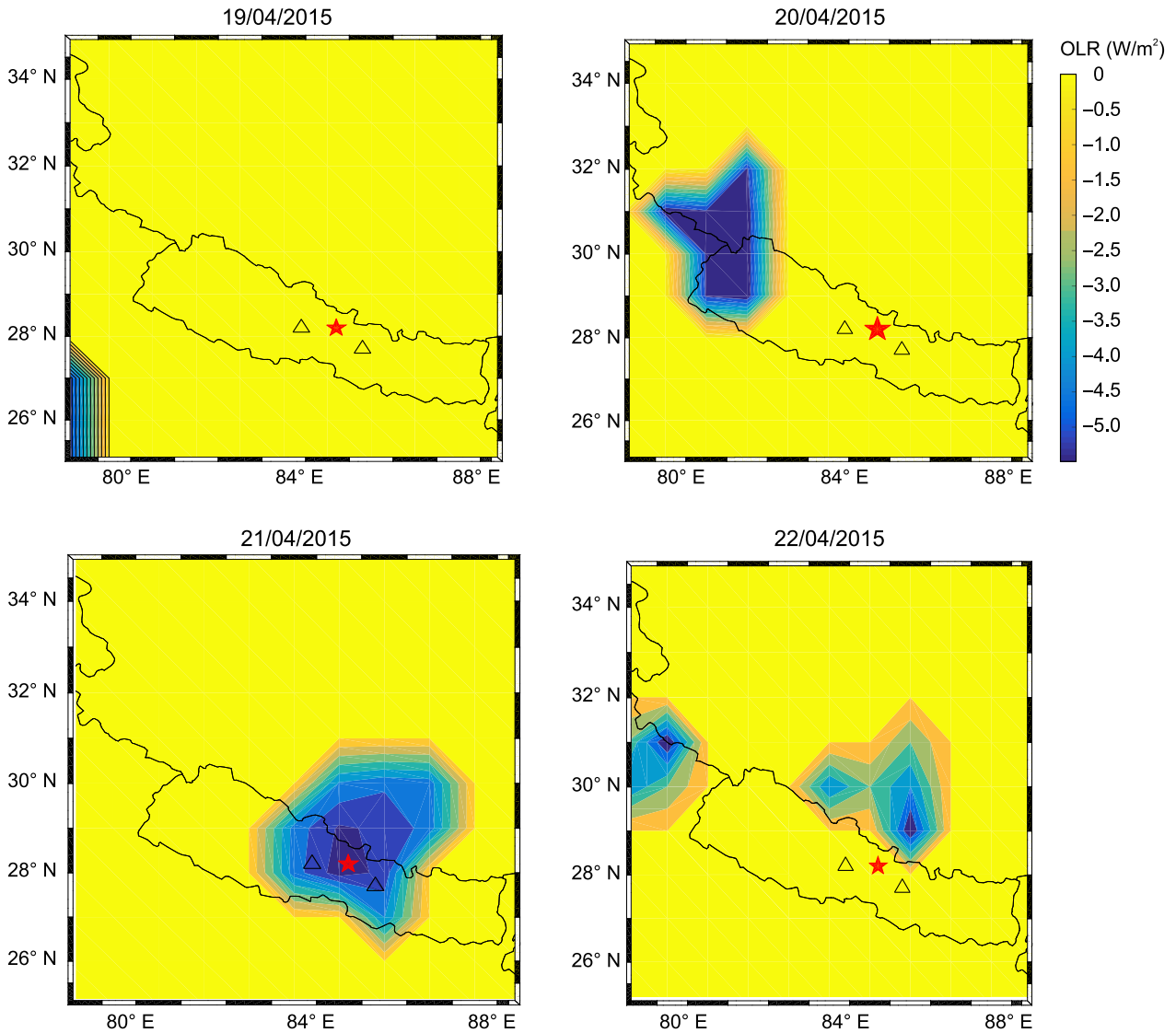


Fig. 9. Spatial pattern of the daily OLR prior to the Mw 7.8 Nepal earthquake. The red star marks the Mw 7.8 earthquake epicenter. The two black triangles show the locations of Pokhara and Kathmandu cities.

Рис. 9. Пространственные изменения суточных значений OLR накануне Непальского землетрясения Mw=7.8. Красной звездочкой отмечен эпицентр землетрясения (Mw=7.8). Два черных треугольника показывают местоположение городов Покхара и Катманду.

the lower atmosphere to the east. The size of this OLR anomaly is $5 \times 3^\circ$ (Longitude \times Latitude), which is close to the size of the MODIS anomaly.

There is no other reliable tool to monitor thermal perturbations in the atmosphere other than the satellite instruments. The observations presented in this case study provide a stringent clue to guide us to the knowledge of what the thermal anomalies are and how they may form. This study clearly demonstrates that, in all the case studies mentioned here, the pre-earthquake atmospheric anomalies formed along the fault lines. The correlation between MODIS and OLR suggests that the thermal anomalies are linked to an impending earthquake. The OLR anomalies can provide important

information about the chemistry of the upper atmosphere. The OLR images mentioned above indicate, that most of the energy accumulated west of the epicenter gradually shifted to eastward, following the Main Boundary Thrust (MBT). This is another evidence that the energy evolved from the seismogenic zone.

3.3. DISCUSSION

In this case study, the pre-earthquake thermal anomalies were examined from the MODIS LST and OLR data using the statistical and mathematical methods. These physical parameters showed abnormal characteristics in the lithosphere and subsequently, in the at-

mosphere prior to the main shock that hit on 25 April 2015. The atmospheric temperature values obtained from the nearby meteorological stations also show the perturbations prior and after the Mw 7.8 earthquake. The anomalous atmospheric temperature was indicative of the absence of a cloud cover on the seismogenic zone. The traveling thermal anomalies in the absence of a cloud might be due to the huge thrust of ions and hole charges from the epicenter of the impending earthquake. As shown in Table 1, four aftershocks of Mw>6 were recorded after the main shock of Mw=7.8. This could justify the existence of a huge amount of energy over the epicenter following the Mw=7.8.

The TIR anomalies and their association with the earthquake in hilly terrain areas, like those in our case study, have more uncertainties. However, the anomalous features in atmospheric temperature and OLR are supporting LST abnormalities. The LST images were used in [Piroddi et al., 2014a; 2014b] for the detection of TIR anomalies in the hilly terrain region hit by the M 6.3 L'Aquila earthquake. However, Figure 1b of Piroddi et al. [2014a] does not show significant TIR anomalies over the epicenter, which is a controversy over the theory of hot gases emission from the earthquake breeding zone. However, it illustrates the association of the TIR anomalies with the earthquake surrounding areas. They further identified the enhanced thermal gradient of TIR around the epicenter in the nighttime section. On the other hand, Cervone et al. [2006] found thermal anomalies before some coastal earthquakes. Based on the wavelet transformation of the long-term LST data, they showed the vulnerable zones in the atmosphere over the epicenter before the impending earthquake. The credibility of the lithosphere for the generation of TIR anomalies was discussed in [Cervone et al., 2006; Saraf et al., 2008; Zhou et al., 2010].

In this study, a significant enhancement in LST is seen 5 days prior to the earthquake. The statistical result is further confirmed by the wavelet density spectrum as well as the spatial images of MODIS LST. All the analysis of LST showed an anomaly of 10–15 °C in the atmosphere above the epicenter. The TIR anomalies of 5–7 °C and 6–10 °C were detected by Saraf et al. [2008]. In order to provide a stringent proof to LST anomalies, the OLR data over Nepal was consolidated and analyzed. The spiky peak of the daily averaged OLR data on amounts to 32 W/m² on 21 April 2015, which is more than 10 W/m² higher than the usual distribution. The OLR data analysis shows that thermal anomalies are traveling along the fault line from the 19th to 22nd of April prior to the earthquake.

A number of studies [e.g. Kang et al., 2008; Ouzounov et al., 2007] suggests a correlation between the OLR perturbations and seismic events. A significant enhancement in LST and OLR, which is detected by both spa-

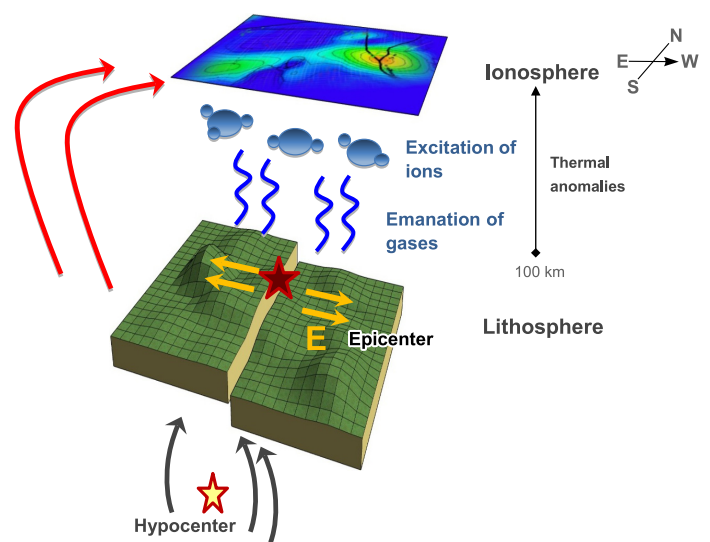


Fig. 10. An assumed configuration of thermal anomalies in the atmosphere between the lithosphere and the ionosphere. This assumption is based on the previous findings published in [Freund, 2000; Pulinets, Ouzounov, 2011].

Рис. 10. Предполагаемая конфигурация тепловых аномалий в атмосфере между литосферой и ионосферой. Предположение основано на выводах, опубликованных в [Freund, 2000; Pulinets, Ouzounov, 2011].

tial and temporal analysis, may be due to the ions from the earthquake breeding zone. The mechanism of the generation of OLR anomalies before the earthquake under the lithosphere-atmosphere coupling model was discussed by Kang et al. [2008]. Ouzounov et al. [2007] also illustrated the TIR anomalies by using OLR data before some major earthquakes. They proposed the earthquake as the source for the eastward drift of OLR anomalies. In their case study, the unusual OLR value is also travelling eastward over the seismogenic zone.

As shown in Fig. 10, the TIR and ionospheric anomalies are portrayed in association with the earthquake. The idea of Fig. 10 was taken from the previous findings of [Pulinets et al., 2006b; Freund, 2010]. The definition of earthquake-induced atmospheric anomalies is as follows: the generation of hole charges at the lithosphere and the intensification of the lower atmosphere by the hole charges.

A number of theories and models have been proposed to explain thermal anomalies caused by stress rock along the tectonic lineaments on the Earth surface [e.g., Freund, 2010; Kuo et al., 2011; Pulinets, Ouzounov, 2011]. The indispensable definition for the generation of thermal anomalies is the release of hole charges from the rocks, which are subjected to stress [Freund, 2010]. Rocks under stress can generate more and more hole charges during the earthquake preparation period. These surface charges distribute in the surrounding

atmosphere around the earthquake epicenter. Apart from this, the complex reaction between the surface charges and light ions in the atmosphere may cause TIR anomalies.

Pulinets and *Ouzonov* [2011] presented a model named LIAC showing the connection between the anomalies in the lithosphere and atmosphere and the evolution of atmospheric anomalies. Recently, *Kuo et al.* [2011] formulated a coupling model for the stressed rock – Earth surface charges – atmosphere – ionosphere system. It was shown that the earthquake-induced hole charges are involved in the generation of seismic atmospheric anomalies. These hole charges may cause the thermal anomalies, which may produce vertical electric fields in the ionosphere. In our case study, the thermal anomalies detected from the MODIS and OLR measurement data may be due to the Mw 7.8 earthquake but an explicit relation has not yet been revealed. It is challenging to gain a complete understanding of the mechanism for the lithosphere – atmosphere coupling, which still needs more investigation.

4. CONCLUSION

The instantaneous enhancement in different atmospheric constituent ions prior to the Mw 7.8 Nepal

earthquake demonstrates that the occurrence of such anomalies may be a precursor of an impending earthquake, while other geophysical events cannot generate such perturbations. Our case study shows that the ground and satellite temperature, as well as OLR measurement datasets can provide a comprehensive platform to study the seismic anomalies and the characteristics of tiny particles raised from the earthquake breeding zone. It was revealed that the MODIS LST and OLR anomalies strictly follow the fault plane. It means that thermal anomalies are detectable along the seismogenic zones. Another interesting thing discovered is that the Earth surface temperature and the OLR anomalies formed dense clouds around the epicenter 10 days before the earthquake. The anomalies in surface temperature and OLR can provide insights about the future earthquake, however, more work need to prove the mechanism.

5. ACKNOWLEDGMENTS

The authors are very grateful to NASA, NOAA/AVHRR and USGS for providing the MODIS LST, OLR and earthquake data, respectively. We are also thankful to weather stations in Pokhara and Kathmandu, as well as the Nepal Geological Survey for their valuable data.

6. REFERENCES

- Akhoondzadeh M.*, 2012. Anomalous TEC variations associated with the powerful Tohoku earthquake of 11 March 2011. *Natural Hazards and Earth System Sciences* 12 (5), 1453–1462. <https://doi.org/10.5194/nhess-12-1453-2012>.
- Cao M., Qiao P.*, 2008. Integrated wavelet transform and its application to vibration mode shapes for the damage detection of beam-type structures. *Smart Materials and Structures* 17 (5), 055014. <https://doi.org/10.1088/0964-1726/17/5/055014>.
- Cervone G., Maekawa S., Singh R. P., Hayakawa M., Kafatos M., Shvets A.*, 2006. Surface latent heat flux and nighttime LF anomalies prior to the Mw=8.3 Tokachi-Oki earthquake. *Natural Hazards and Earth System Science* 6 (1), 109–114. <https://doi.org/10.5194/nhess-6-109-2006>.
- Freund F.*, 2000. Time-resolved study of charge generation and propagation in igneous rocks. *Journal of Geophysical Research: Solid Earth* 105 (B5), 11001–11019. <https://doi.org/10.1029/1999JB900423>.
- Freund F.*, 2003. Rocks that crackle and sparkle and glow: strange pre-earthquake phenomena. *Journal of Scientific Exploration* 17 (1), 37–71.
- Freund F.*, 2010. Toward a unified solid state theory for pre-earthquake signals. *Acta Geophysica* 58 (5), 719–766. <https://doi.org/10.2478/s11600-009-0066-x>.
- Freund F., Takeuchi A., Lau B.W.S., Al-Manaseer A., Fu C.C., Byrant N.A., Ozounov D.*, 2007. Stimulated infrared emission from rocks: assessing a stress indicator. *eEarth* 2 (1), 7–16.
- Grinsted A., Moore J., Jevrejeva S.*, 2004. Application of the cross wavelet transform and wavelet coherence to geophysical time series. *Nonlinear Processes in Geophysics* 11 (5–6), 561–566. <https://doi.org/10.5194/npg-11-561-2004>.
- He L.M., Wu L.X., De Santis A., Liu S.J., Yang Y.*, 2014. Is there a one-to-one correspondence between ionospheric anomalies and large earthquakes along Longmenshan faults? *Annales Geophysicae* 32 (2), 187–196. <https://doi.org/10.5194/angeo-32-187-2014>.
- Jianxi H., Feng M., Wensheng Z., Xianlong Z.*, 2008. Satellite thermal IR associated with Wenchuan earthquake in China using MODIS data. In: Proceedings of the 14th World Conference on Earthquake Engineering (October 12–17, 2008, Beijing, China), p. 12–17.
- Jin S.G., Occhipinti G., Jin R.*, 2015. GNSS ionospheric seismology: Recent observation evidences and characteristics. *Earth-Science Reviews* 147, 54–64. <https://doi.org/10.1016/j.earscirev.2015.05.003>.

- Jin S.G., Zhu W.Y., Afraimovich E., 2010. Co-seismic ionospheric and deformation signals on the 2008 magnitude 8.0 Wenchuan Earthquake from GPS observations. *International Journal of Remote Sensing* 31 (13), 3535–3543. <https://doi.org/10.1080/01431161003727739>.
- Kang C.L., Han Y.B., Liu D.F., Cao Z.Q., 2008. The OLR anomaly and mechanism before Tibet earthquake M 6.9. *Progress in Geophysics* 6, 1703–1708 (in Chinese with English abstract).
- Kuo C.L., Huba J.D., Joyce G., Lee L.C., 2011. Ionosphere plasma bubbles and density variations induced by pre-earthquake rock currents and associated surface charges. *Journal of Geophysical Research: Space Physics* 116 (A10), A10317. <https://doi.org/10.1029/2011JA016628>.
- Liebmann B., 1996. Description of a complete (interpolated) outgoing long wave radiation dataset. *Bulletin of the American Meteorological Society* 77 (6), 1275–1277.
- Liperovsky V.A., Meister C.V., Liperovskaya E.V., Vasil'eva N.E., Alimov O., 2005. On spread-Es effects in the ionosphere before earthquakes. *Natural Hazards and Earth System Science* 5 (1), 59–62. <https://doi.org/10.5194/nhess-5-59-2005>.
- Liu J.Y., Chen Y.I., Chen C.H., Liu C.Y., Chen C.Y., Nishihashi M., Li J.Z., Xia Y.Q., Oyama K.I., Hattori K., Lin C.H., 2009. Seismoionospheric GPS total electron content anomalies observed before the 12 May 2008 Mw 7.9 Wenchuan earthquake. *Journal of Geophysical Research: Space Physics* 114 (A4), A04320. <https://doi.org/10.1029/2008JA013698>.
- Ouzounov D., Liu D., Chunli K., Cervone G., Kafatos M., Taylor P., 2007. Outgoing long wave radiation variability from IR satellite data prior to major earthquakes. *Tectonophysics* 431 (1–4), 211–220. <https://doi.org/10.1016/j.tecto.2006.05.042>.
- Piroddi L., Ranieri G., Freund F.T., Trogu A., 2014a. TIR, tectonics and geology in L'Aquila 2009. In: *Proceeding of Electromagnetic Studies of Earthquakes and Volcanoes (EMSEV) 2014*, Warsaw, Poland, p. 37–40.
- Piroddi L., Ranieri G., Freund F.T., Trogu A., 2014b. Geology, tectonics and topography underlined by L'Aquila earthquake TIR precursors. *Geophysical Journal International* 197 (3), 1532–1536. <https://doi.org/10.1093/gji/ggu123>.
- Přša D., Parrot M., Santolík O., 2011. Ionospheric density variations recorded before the 2010 Mw 8.8 earthquake in Chile. *Journal of Geophysical Research: Space Physics* 116 (A8), A08309. <https://doi.org/10.1029/2011JA016611>.
- Pulinets S., Ouzounov D., 2011. Lithosphere – Atmosphere – Ionosphere Coupling (LAIC) model – An unified concept for earthquake precursors validation. *Journal of Asian Earth Sciences* 41 (4–5), 371–382. <https://doi.org/10.1016/j.jseaes.2010.03.005>.
- Pulinets S.A., Ouzounov D., Ciraolo L., Singh R., Cervone G., Leyva A., Dunajacka M., Karelin A.V., Boyarchuk K.A., Kotsarenko A., 2006b. Thermal, atmospheric and ionospheric anomalies around the time of the Colima M 7.8 earthquake of 21 January 2003. *Annales Geophysicae* 24 (3), 835–849. <https://doi.org/10.5194/angeo-24-835-2006>.
- Qin K., Wu L.X., De Santis A., Meng J., Ma W.Y., Cianchini G., 2012. Quasi-synchronous multi-parameter anomalies associated with the 2010–2011 New Zealand earthquake sequence. *Natural Hazards and Earth System Sciences* 12 (4), 1059–1072. <https://doi.org/10.5194/nhess-12-1059-2012>.
- Rawat V., Saraf A.K., Das J., Sharma K., Shujat Y., 2011. Anomalous land surface temperature and outgoing long-wave radiation observations prior to earthquakes in India and Romania. *Natural Hazards* 59 (1), 33–46. <https://doi.org/10.1007/s11069-011-9736-5>.
- Saradjian M.R., Akhoondzadeh M., 2011. Thermal anomalies detection before strong earthquakes (Mw>6.0) using interquartile, wavelet and Kalmanfilter methods. *Natural Hazards and Earth System Sciences* 11(4), 1099–1108. <https://doi.org/10.5194/nhess-11-1099-2011>.
- Saraf A.K., Rawat V., Banerjee P., Choudhury S., Panda S.K., Dasgupta S., Das J.D., 2008. Satellite detection of earthquake thermal infrared precursors in Iran. *Natural Hazards* 47 (1), 119–135. <https://doi.org/10.1007/s11069-007-9201-7>.
- Shah M., Jin S.G., 2015. Statistical characteristics of seismo-ionospheric GPS TEC disturbances prior to global Mw>5.0 earthquakes (1998–2014). *Journal of Geodynamics* 92, 42–49. <https://doi.org/10.1016/j.jog.2015.10.002>.
- Tronin A.A., Biagi P.F., Molchanov O.A., Khatkevich Y.M., Gordeev E.I., 2004. Temperature variations related to earthquakes from simultaneous observation at the ground stations and by satellites in Kamchatka area. *Physics and Chemistry of the Earth, Parts A/B/C* 29 (4–9), 501–506. <https://doi.org/10.1016/j.pce.2003.09.024>.
- Xiong P., Shen X.H., Bi Y.X., Kang C.L., Chen L.Z., Jing F., Chen Y., 2010. Study of outgoing longwave radiation anomalies associated with Haiti earthquake. *Natural Hazards and Earth System Sciences* 10 (10), 2169–2178. <https://doi.org/10.5194/nhess-10-2169-2010>.
- Zhang X., Shen X., Liu J., Ouyang X., Qian J., Zhao S., 2009. Analysis of ionospheric plasma perturbations before Wenchuan earthquake. *Natural Hazards and Earth System Sciences* 9 (4), 1259–1266. <https://doi.org/10.5194/nhess-9-1259-2009>.
- Zhou X., Du J., Chen Z., Cheng J., Tang Y., Yang L., Xie C., Cui Y., Liu L., Yi L., 2010. Geochemistry of soil gas in the seismic fault zone produced by the Wenchuan Ms 8.0 earthquake, southwestern China. *Geochemical Transactions* 11 (1), Article 5. <https://doi.org/10.1186/1467-4866-11-5>.



Munawar Shah, PhD
Women University Swabi
Guloo Dehri, Swabi, Khyber Pakhtunkhwa, Pakistan
✉ e-mail: shahmunawar1@gmail.com; shahmunawar12@yahoo.com



Majid Khan, PhD
University of Chinese Academy of Sciences
University of Chinese Academy of Sciences, Beijing 100047, China
e-mail: majidkktk.000@gmail.com



Hafeez Ullah, PhD
Quaid-i-Azam University
Quaid-i-Azam University, Islamabad, Pakistan
e-mail: hafeezllh496@gmail.com



Sajjad Ali, PhD
Quaid-i-Azam University
Quaid-i-Azam University, Islamabad, Pakistan
e-mail: Sajjadalikhan21@gmail.com